Clinical Evaluation of Deep Learning–Reconstructed Readout-Segmented Diffusion-Weighted Imaging with Water-Excitation-Spectral Fat Suppression in 3T Breast MRI

Jung Min Choi , Soyeoun Lim , Eun Jung Choi , MunYoung Paek , Wei Liu , Minseo Bang * , Jung Hee Byon *

Posted Date: 22 May 2026

doi: 10.20944/preprints202605.1478.v1

Keywords: diffusion magnetic resonance imaging; echo-planar imaging; deep learning; fat suppression; breast neoplasms

 doi:10.20944/preprints202605.1478.v1

Article

Clinical Evaluation of Deep Learning–Reconstructed Readout-Segmented Diffusion-Weighted Imaging with Water-Excitation-Spectral Fat Suppression in 3T Breast MRI

Jung Min Choi [1], Soyeoun Lim [1], Eun Jung Choi [2], MunYoung Paek [3], Wei Liu [4], Minseo Banga [1,*] and Jung Hee Byona [1,*]

[1] Department of Radiology, Ulsan University Hospital, University of Ulsan College of Medicine, Ulsan, Republic of Korea

[2] Department of Radiology, Research Institute of Clinical Medicine of Jeonbuk National University-Biomedical Research Institute of Jeonbuk National University Hospital, Jeonbuk National University Medical School, Jeonju, Korea

[3] Siemens Healthineers Ltd., Seoul, Republic of Korea

[4] Siemens Healthineers AG, Erlangen, Germany

* Correspondence: bangms@uuh.ulsan.kr (M.B.); 0736359@uuh.ulsan.kr (J.H.B.)

Abstract

Objectives: To evaluate whether deep-learning–reconstructed readout-segmented echo-planar imaging (DL-rs-EPI) with combined water-excitation-spectral-fatsat (WEXfs) improves image quality compared with conventional rs-EPI using spectral attenuated inversion recovery at 3 T. **Methods**: Overall, 80 patients underwent breast magnetic resonance imaging (MRI) with conventional and DL-rs-EPI using WEXfs techniques (b-values: 0, 800, and 1200 s/mm²). Signal-to-noise ratio (SNR), contrast-to-noise ratio (CNR), and lesion contrast were assessed at b = 800 and b = 1200; apparent diffusion coefficient (ADC) was calculated using multi-b data. Fat suppression, background diffusion signal, lesion conspicuity, and artifact severity were qualitatively evaluated. A temperature-controlled diffusion phantom (CaliberMRI) was scanned; ADC values were compared with reference values at 24°C. **Results**: DL-rs-EPI with WEXfs demonstrated high SNR (b800: 5.79 vs 5.28; b1200: 5.41 vs 4.94; $p<0.001$) and CNR (b800: 3.35 vs 3.12, $p = 0.024$; b1200: 3.67 vs 3.37, $p = 0.001$), with unchanged lesion contrast. Tumor ADC values were comparable between methods, whereas normal tissue ADC values were slightly higher, and ADC contrast increased with DL-rs-EPI with WEXfs. Phantom ADCs from both protocols closely matched reference values at 24°C, without significant differences. DL-rs-EPI with WEXfs demonstrated greater homogeneous fat suppression and reduced background diffusion signal, with comparable lesion conspicuity and artifact severity. **Conclusions**: DL–rs-EPI with WEXfs improved image quality while preserving diffusion metrics, supporting its clinical feasibility.

Keywords: diffusion magnetic resonance imaging; echo-planar imaging; deep learning; fat suppression; breast neoplasms

1. Introduction

Breast cancer remains highly prevalent worldwide, contributing to the increasing use of breast magnetic resonance imaging (MRI) [1–3]. Dynamic contrast-enhanced (DCE) T1-weighted imaging (T1WI) remains the cornerstone of breast MRI protocols [4]. In parallel, diffusion-weighted imaging (DWI) has increasingly been incorporated into multiparametric breast MRI as a complementary

 doi:10.20944/preprints202605.1478.v1

technique providing functional information without contrast agents [5]. Consequently, interest in non-contrast MRI, particularly DWI, has continued to grow [5].

Contemporary consensus statements describe breast DWI as commonly performed using echo-planar imaging (EPI)-based readout strategies [6,7]. Single-shot EPI (ss-EPI) acquires all k-space lines for a given slice within a single excitation, enabling rapid image acquisition (50–100 ms per slice) and reducing sensitivity to patient motion [7]. However, the long echo train inherent to ss-EPI makes it highly susceptible to T2* decay and magnetic field inhomogeneity, leading to geometric distortion, image blurring, and consequently limited spatial resolution [5,7]. To overcome these limitations, multi-shot EPI techniques have been introduced by segmenting k-space acquisition across multiple excitations. Multi-shot EPI techniques, such as readout-segmented EPI (rs-EPI), divide k-space acquisition into multiple segments along the readout direction, thereby shortening the echo train length and the echo spacing. This approach reduces susceptibility-induced geometric distortion and image blurring, enabling higher spatial resolution compared with ss-EPI [5,7]. Deep learning (DL)-based reconstruction has recently been introduced as a vendor-implemented approach that may improve image appearance and noise performance in diffusion MRI [8,9]. Although previous studies have investigated DL reconstruction in single-shot [8,9] or alternative multi-shot diffusion techniques [10], its clinical performance within an rs-EPI protocol for breast MRI remains insufficiently analyzed.

Another key technical consideration in breast DWI is fat suppression. Given that low apparent diffusion coefficient (ADC) values are an important imaging feature suggestive of malignancy, fat contamination can spuriously reduce ADC measurements and increase false-positive findings. Accordingly, several organizations—including the European Society of Breast Imaging [6], Quantitative Imaging Biomarkers Alliance/Radiological Society of North America [11], and the Korean Radiological Society [7]—recommend spectral attenuated inversion recovery (SPAIR) as the preferred fat-suppression technique for breast DWI. SPAIR is more robust to B1 inhomogeneities than spectral fat saturation and provides a higher signal-to-noise ratio (SNR) compared to short inversion time inversion recovery. However, a recent report suggested that combining water excitation (WEX), which selectively excites water protons, with spectral fat saturation may provide superior image quality compared with SPAIR in breast DWI by improving robustness to B1 inhomogeneities [12]. Notably, this comparison was performed in ss-EPI–based breast DWI rather than rs-EPI, and evidence specific to rs-EPI breast DWI remains limited.

Therefore, this study aimed to evaluate the image quality and quantitative diffusion metrics of a clinically available DL-rs-EPI DWI with water-excitation-spectral-fatsat (WEXfs) protocol compared with a conventional rs-EPI protocol with SPAIR at 3T.

 doi:10.20944/preprints202605.1478.v1

2. Materials and Methods

2.1. Study Design and Patients

This single-center, retrospective study was conducted at Ulsan University Hospital. The Institutional Review Board (IRB) approved this study, and the requirement for informed consent was waived (IRB No. 2025-09-022). Between July 22, 2024, and February 10, 2025, a total of 326 patients underwent breast MRI for breast cancer diagnosis. Patients were eligible for inclusion if they (i) had pathologically confirmed breast cancer and (ii) underwent breast MRI in a single session, including both conventional rs-EPI and DL-rs-EPI with WEXfs. Patients were excluded if they met any of the following criteria: (i) neoadjuvant chemotherapy before MRI; (ii) excisional biopsy performed before the MRI; (iii) absence of a clearly visible index breast malignancy on MRI, precluding qualitative scoring; (iv) absence or insufficiency of normal breast parenchyma for standardized comparisons due to a history of contralateral mastectomy or male breast cancer; (v) technical failure or acquisition error affecting either the conventional rs-EPI or DL-rs-EPI with WEXfs sequences; or (vi) incomplete clinical or pathological data.

2.2. MRI Acquisition

All examinations were performed using a 3-T MR scanner (MAGNETOM Vida; Siemens Healthineers, Forchheim, Germany) with a dedicated 18-channel phased-array breast coil, with patients in the prone position. The breast MRI protocol included fat-saturated T2-weighted turbo spin-echo imaging and two DWI sequences (conventional rs-EPI and DL-rs-EPI with WEXfs), followed by five phases of DCE T1WI after intravenous administration of a gadolinium-based contrast agent (Dotarem; Guerbet, Paris, France). The acquisition parameters for the two DWI sequences are summarized in Table 1.

Table 1. Scan parameters of two sequences of diffusion-weighted imaging.

Scan Parameters	**rs-EPI**	**DL-rs-EPI**
TR/TE1/TE2 (ms)	5760/61/100	5000/61/100
Slice thickness (mm)/Number of slices/Slice gap (mm)	3/50/0	3/50/0
FOV (mm^2)	320 x 192	320 x 192
Matrix size	220 x 220	220 x 220
In-plane resolution (mm^2)	0.7 × 0.7	0.7 × 0.7
Acceleration factor	2 (SMS), 2 (GRAPPA)	2 (SMS), 2 (GRAPPA)
Readout partial Fourier	7/8	7/8
Readout Segments	5	5
b-value (s/mm^2)	0, 800, 1200	0, 800, 1200
NEX per b-value	1, 1, 2	1, 1, 2
Receiver Bandwidth (Hz/px)	947	947
Fat suppression	SPAIR	WEX (water excitation)
Acquisition time (min: sec)	04:35	04:00

※ rs-EPI, readout-segmented echo-planar imaging; DL-rs-EPI, deep learning–based reconstruction applied to rs-EPI; TR, repetition time; TE1/TE2, first/second echo time; FOV, field of view; in-plane resolution, pixel size; SMS, simultaneous multi-slice; GRAPPA, Generalized Autocalibrating Partially Parallel Acquisition; readout partial Fourier, fraction of k-space sampled in readout; readout segments, number of readout shots; NEX (NSA), number of excitations/averages per b-value; Hz/px, Hz per pixel; SPAIR, spectral attenuated inversion recovery; WEX, water-excitation-spectral-fatsat method.

 doi:10.20944/preprints202605.1478.v1

2.3. DL-Based MR Image Reconstruction

DL-rs-EPI images were reconstructed using a DL reconstruction framework integrated into a prototype rs-EPI diffusion sequence. The network was based on a variational network architecture with 17 unrolled iterations [13] and operated directly on raw k-space data together with pre-calculated coil sensitivity maps, which were estimated using vendor-provided autocalibration data. The model was trained in a supervised manner using a large DWI dataset acquired on 1.5-T and 3-T MR systems (MAGNETOM, Siemens Healthineers, Forchheim, Germany), and the final network was implemented for inline reconstruction on the scanner. The DL reconstruction framework with WEXfs, which has previously been demonstrated for abdominal DWI [14], was adapted for rs-EPI by incorporating dedicated phase-correction and segment-combination steps, ensuring compatibility with the rs-EPI sequence [15].

2.4. Fat Suppression Technique

For EPI-based DWI, reliable fat suppression is essential to minimize chemical shift-related ghosting and associated image degradation. In the conventional rs-EPI DWI protocol, SPAIR was employed for fat suppression due to its robustness to B0 and B1 inhomogeneities. In the prototype DL-rs-EPI DWI protocol, WEXfs was applied. In this implementation, the conventional adiabatic inversion pulse used in SPAIR was omitted, and a spectrally selective sinc-shaped fat-saturation radiofrequency pulse was utilized instead. In addition, the excitation module was replaced with a WEX sequence employing a monopolar 1-2-2-1 composite scheme designed to preferentially excite water while minimizing fat excitation, thereby improving the robustness of fat suppression. The WEXfs configuration was integrated into the rs-EPI diffusion acquisition and was compatible with simultaneous multi-slice acceleration.

2.5. Qualitative Image Analysis

Two dedicated breast radiologists (with 8 and 10 years of experience in breast MRI interpretation) independently performed qualitative image assessments while blinded to the DWI sequence type and reconstruction method. For each examination, overall image quality was graded using predefined ordinal scales. Homogeneity of fat suppression was rated on a four-point scale (1 = failure of fat suppression, 2 = regional failure but still interpretable, 3 = minimal failure limited to the image periphery, 4 = homogeneous fat suppression); background diffusion signal was scored on a 1–4 scale (1 = minimal, 2 = mild, 3 = moderate, 4 = marked); and lesion conspicuity was scored on a 1–3 scale (1 = poor, 2 = moderate, 3 = excellent). Furthermore, artifact severity was recorded on a 0–3 scale (0 = none, 1 = mild, 2 = moderate, 3 = severe), considering susceptibility-related distortion, aliasing, and misregistration artifacts, with emphasis on their overall impact on image interpretability. Qualitative parameters were assessed at b-values of 800 and 1200 s/mm².

Qualitative scoring of global image quality parameters (fat suppression and background diffusion signal) was performed on a per-patient basis. Lesion conspicuity was evaluated on a lesion-by-lesion basis. In cases with multiple lesions, the index lesion, defined as the largest lesion with a solid enhancing component, was selected for analysis. Scores were recorded separately for each DWI sequence (DL-rs-EPI with WEXfs and rs-EPI), and inter-reader agreement was subsequently quantified.

2.6. Quantitative Image Analysis

Quantitative measurements were performed for each DWI reconstruction (conventional rs-EPI and DL-rs-EPI with WEXfs) using PACS software. One radiologist performed all measurements twice at each location, and the mean value was used for analysis. For paired comparison, regions of interest (ROIs) were initially delineated on one sequence and subsequently transferred to the corresponding anatomical location on the other sequence.

 doi:10.20944/preprints202605.1478.v1

For each sequence, two manual freehand ROIs were drawn on the high-b-value images to encompass (i) the largest solid component of the index tumor and (ii) normal fibroglandular tissue (FGT). ROIs were consistently placed at matched anatomical locations across both reconstructions and at b-values of 800 and 1200 s/mm². Normal FGT was sampled in the contralateral breast in an area without enhancement on DCE images. Tumor ROIs were delineated along lesion margins while avoiding necrotic or hemorrhagic components, with reference to T2-weighted and DCE images. For non-mass enhancement, ROIs were delineated to follow the enhancing area on DCE images to minimize inclusion of normal FGT. ROI size was maximized within lesion boundaries as far as possible to reduce sampling variability.

For each b-value (800 and 1200 s/mm²), SNR (SI_tumor / σ_tumor), contrast-to-noise ratio (CNR = |SI_tumor − SI_normal| / √(σ_tumor² + σ_normal²)), and lesion contrast (Lesion contrast = SI_tumor / SI_normal) were calculated. Definitions and equations for these metrics were based on a previously published study [9]. Each tumor ROI drawn on the high b-value images was transferred to the co-registered ADC map to obtain tumor ADC values. Normal tissue ADC was measured using the corresponding FGT ROI. ADC contrast was defined a priori as the difference between normal tissue ADC and tumor ADC (ADC_normal − ADC_tumor), expressed in $\times 10^{-3}$ mm²/s.

2.7. Phantom Experiment

A calibrated diffusion phantom (Diffusion Standard Model 128, CaliberMRI, Boulder, CO, USA) was used to assess the accuracy of ADC measurements obtained with the two DWI protocols. Each protocol was acquired using the same imaging parameters as in the patient study. The phantom comprised a spherical shell containing 13 vials (30 mL each) filled with traceable aqueous polyvinylpyrrolidone (PVP) solutions, with concentrations ranging from 0% (water reference) to 50%. A built-in ten-element liquid-crystal thermometer was used for MR-readable temperature monitoring, enabling temperature compensation over a range of 15–24°C, for which manufacturer-supplied temperature-dependent reference ADC values were available.

Immediately before and after the DWI acquisitions, a three-dimensional Volumetric Interpolated Breath-hold Examination (VIBE) sequence with 1-mm isotropic resolution was acquired to document the phantom temperature and assess potential temperature drift during imaging. For each protocol and PVP vial, one radiologist placed circular ROIs on the PACS workstation to measure ADC values. Measurements were performed twice and averaged for analysis. Protocol comparisons were performed against the temperature-matched reference ADC values for each vial.

2.8. Statistical Analysis

Qualitative scores from the two readers were summarized as mean ± standard deviation (SD) and compared between techniques using the Wilcoxon signed-rank test (two-sided, $\alpha = 0.05$). Inter-reader agreement for qualitative ordinal ratings was assessed using weighted kappa (κ) statistics with 95% confidence intervals (CIs). The κ values were interpreted as follows: 0.00–0.20, poor agreement; 0.21–0.40, fair agreement; 0.41–0.60, moderate agreement; 0.61–0.80, good agreement; and 0.81–1.00, excellent agreement. Quantitative metrics, including SNR, CNR, lesion contrast, ADC values, and ADC contrast, were summarized as mean ± SD and compared using paired t-tests (two-sided, $\alpha = 0.05$) after verification of normality of within-pair differences; where this assumption was violated, the Wilcoxon signed-rank test was performed. Unadjusted p-values are presented for primary paired comparisons unless otherwise specified. All statistical analyses were performed using SPSS version 20.0 (IBM Corp., Armonk, NY, USA).

 doi:10.20944/preprints202605.1478.v1

3. Results

3.1. Characteristics of Patients and Lesions

Among 326 patients, 192 had pathologically confirmed breast cancer and were examined using both DWI sequences. Patients were excluded for any of the following: (i) prior neoadjuvant chemotherapy (n = 72); (ii) excisional biopsy before MRI (n = 20); (iii) absence of a clearly visible index breast malignancy (n = 8); (iv) insufficient normal breast parenchyma (n = 6); (v) technical failure or acquisition error (n = 1); (vi) incomplete clinical or pathology data (n = 5). Consequently, 80 patients were included in this study (Figure 1).

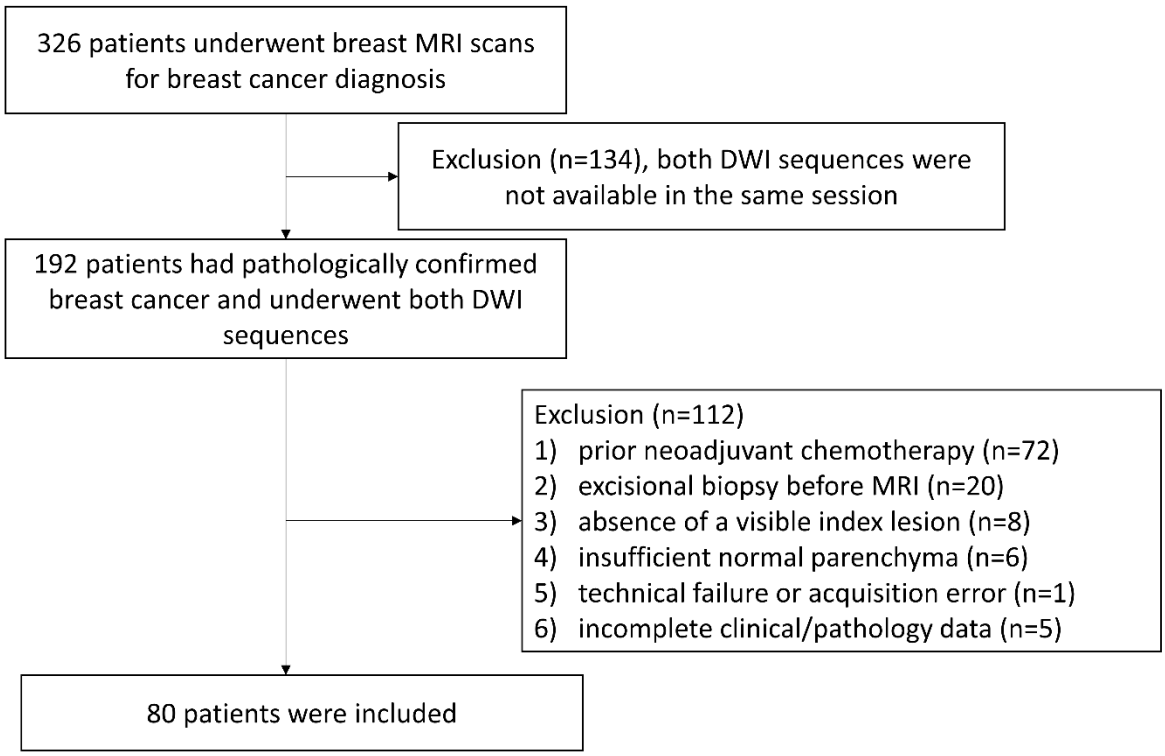

Figure 1. Flow diagram of study sample selection.

The mean age of the 80 women was 55 ± 11 years (range, 25–82 years). In terms of pathology, invasive ductal carcinoma (IDC) was the most common diagnosis (55/80, 68.8%), followed by ductal carcinoma in situ (16/80, 20.0%) and other specific invasive carcinomas (9/80, 11.3%), which included invasive lobular carcinoma (ILC) (n = 5), invasive carcinoma with neuroendocrine differentiation (n = 1), invasive carcinoma with a micropapillary component (n = 1), mixed IDC and ILC (n = 1), and mucinous carcinoma (n = 1). Detailed information on participants and lesion characteristics is presented in Table 2.

Table 2. Patient and lesion characteristics.

Characteristics	Value
Number of patients	80
Age (y)*	55 ± 11 (age range, 25–82)
History of breast cancer	
Absent	80 (100.0)
Present	0 (0.0)
Menopausal status	
Pre-menopause	30 (37.5)
Post-menopause	50 (62.5)
Histology of malignant lesion	

 doi:10.20944/preprints202605.1478.v1

Invasive carcinoma, NOS	55 (68.8)
Invasive carcinoma, other specific type‡	9 (11.3)
DCIS	16 (20.0)
Histologic grade of invasive carcinoma (N = 58) †	
1	11 (19.0)
2	31 (53.4)
3	16 (27.6)
Nuclear grade of DCIS (DCIS N = 16) †	
1	2 (12.5)
2	6 (37.5)
3	8 (50.0)
Predominant lesion on MRI †	
Mass	60 (75.0)
Non-mass	20 (25.0)
Pathologic lesion size, Median (IQR), mm	
All	18.00 (10.5–24.5)
Invasive	15.50 (10.0–23.0)
DCIS	25.00 (13.5–50.5)

※NOS, not otherwise specified; DCIS, ductal carcinoma in situ; IQR, interquartile range; * Data are presented as mean ± standard deviations; medians with interquartile ranges in parentheses. † Values are presented as the number of patients with percentages in parentheses. ‡ "Invasive carcinoma, other specific type" included invasive lobular carcinoma (n = 5), invasive carcinoma with neuroendocrine differentiation (n = 1), invasive carcinoma with micropapillary component (n = 1), mixed invasive ductal carcinoma and invasive lobular carcinoma (n = 1), and mucinous carcinoma (n = 1).

3.2. Phantom Experiment

T1-weighted VIBE imaging confirmed a stable phantom temperature of 24°C throughout the imaging session. Using identical acquisition parameters, the phantom experiment yielded consistent ADC measurements for both conventional rs-EPI and DL-rs-EPI with WEXfs. Representative DWI images and corresponding ADC maps for the two protocols are displayed in Figure 2, demonstrating visually comparable image quality without protocol-specific artifacts.

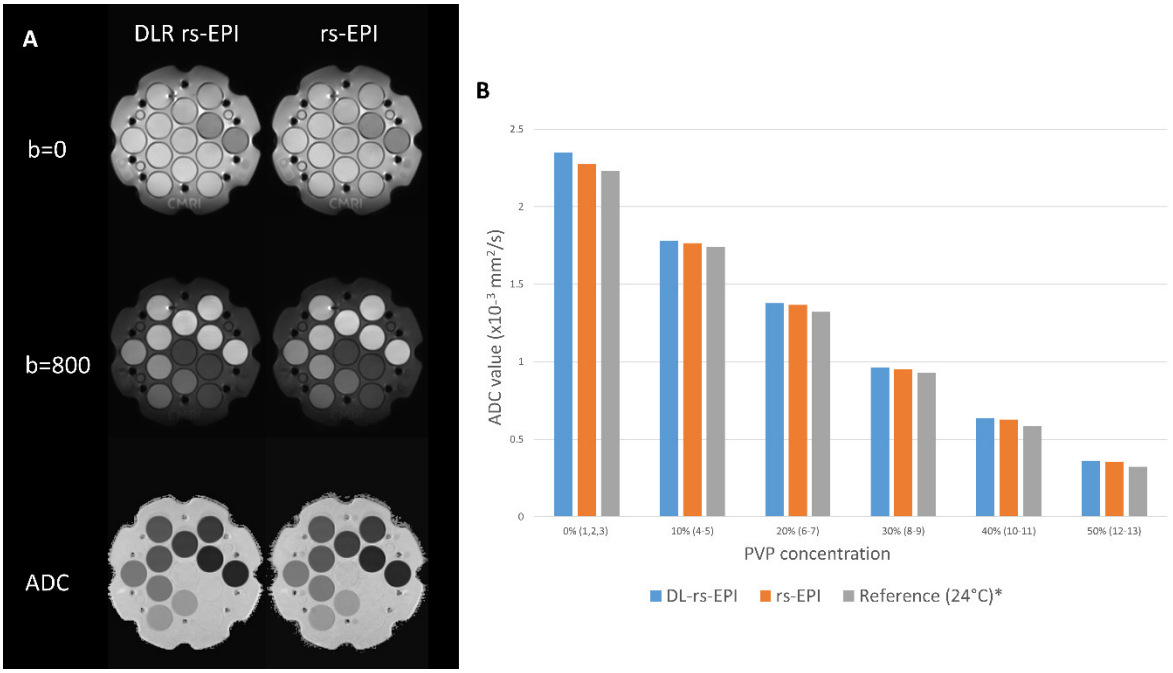

Figure 2. Results of the phantom experiment. (**a**) Diffusion-weighted images (DWI) and corresponding apparent diffusion coefficient (ADC) maps of the DWI phantom for each DWI sequence. ADC values obtained from deep-

 doi:10.20944/preprints202605.1478.v1

learning–reconstructed readout-segmented echo-planar imaging; (**b**) demonstrate no significant differences compared with conventional rs-EPI.

ADC values derived from b-values of 0, 800, and 1200 s/mm² demonstrated no significant differences between protocols across the range of PVP concentrations when circular ROIs were applied. Across all concentrations, measured ADC values exhibited close agreement with the manufacturer-provided reference values at 24°C, with deviations ranging from 1.93% to 12.07%. No significant differences in ADC measurements were observed between conventional rs-EPI and DL-rs-EPI with WEXfs (p = 0.107, Supplementary Table 1).

3.3. Qualitative Analysis and Inter-Reader Agreement

Compared with conventional rs-EPI, DL-rs-EPI with WEXfs demonstrated significantly more homogeneous fat suppression (3.80 ± 0.40 vs 3.25 ± 0.46, p<0.001) (Table 3, Figure 3) and lower background diffusion signal at both b = 800 s/mm² (2.21 ± 1.08 vs 2.30 ± 1.06, p = 0.008) and b = 1200 s/mm² (1.27 ± 0.57 vs 1.58 ± 0.76, p<0.001) (Table 3). In a representative case (Figure 3), conventional rs-EPI (panels a and c) revealed pronounced ghosting artifacts along the phase-encoding direction, likely attributable to shot-to-shot phase inconsistencies and physiologic motion; these artifacts were markedly reduced on DL-rs-EPI with WEXfs (panels b and d). Figure 4 illustrates a representative case demonstrating a diminished background diffusion signal on DL-rs-EPI with WEXfs at b = 1200 s/mm². Lesion conspicuity was comparable between the two sequences at b = 800 s/mm² (2.81 ± 0.48 vs 2.84 ± 0.46, p = 0.317) and b = 1200 s/mm² (2.76 ± 0.56 vs 2.76 ± 0.56, p = 1.000). Artifact severity tended to be lower with DL-rs-EPI with WEXfs (0.65 ± 0.78 vs 0.76 ± 0.90), although this difference was not statistically significant (p = 0.088) (Table 3).

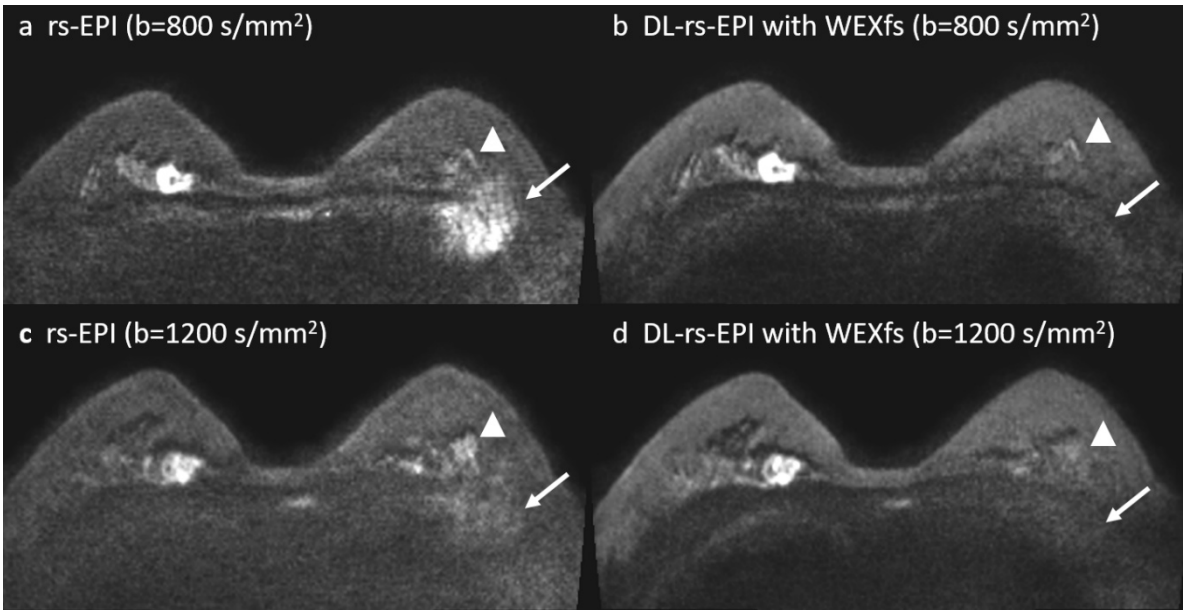

Figure 3. Breast magnetic resonance images of a 46-year-old woman with a 2.6 cm invasive ductal carcinoma (IDC) in the right breast, appearing as a mass lesion. Deep-learning–reconstructed readout-segmented echo-planar imaging (DL-rs-EPI) with water-excitation spectral fat suppression (WEXfs) demonstrated more homogeneous fat suppression with reduced image noise. Conventional rs-EPI diffusion-weighted images display pronounced ghosting artifacts along the phase-encoding direction, likely related to shot-to-shot phase inconsistencies and physiologic motion (arrows in a and c). These artifacts are markedly reduced on the DL-rs-EPI with WEXfs images (arrows in b and d). Background diffusion signal anterior to the sternum was reduced on DL-rs-EPI with WEXfs (arrowheads in b and d) compared with rs-EPI (arrowheads in a and c). The ADC value of the IDC was 0.816 × 10^{-3} mm²/s on rs-EPI and 0.839 × 10^{-3} mm²/s on DL-rs-EPI.

 doi:10.20944/preprints202605.1478.v1

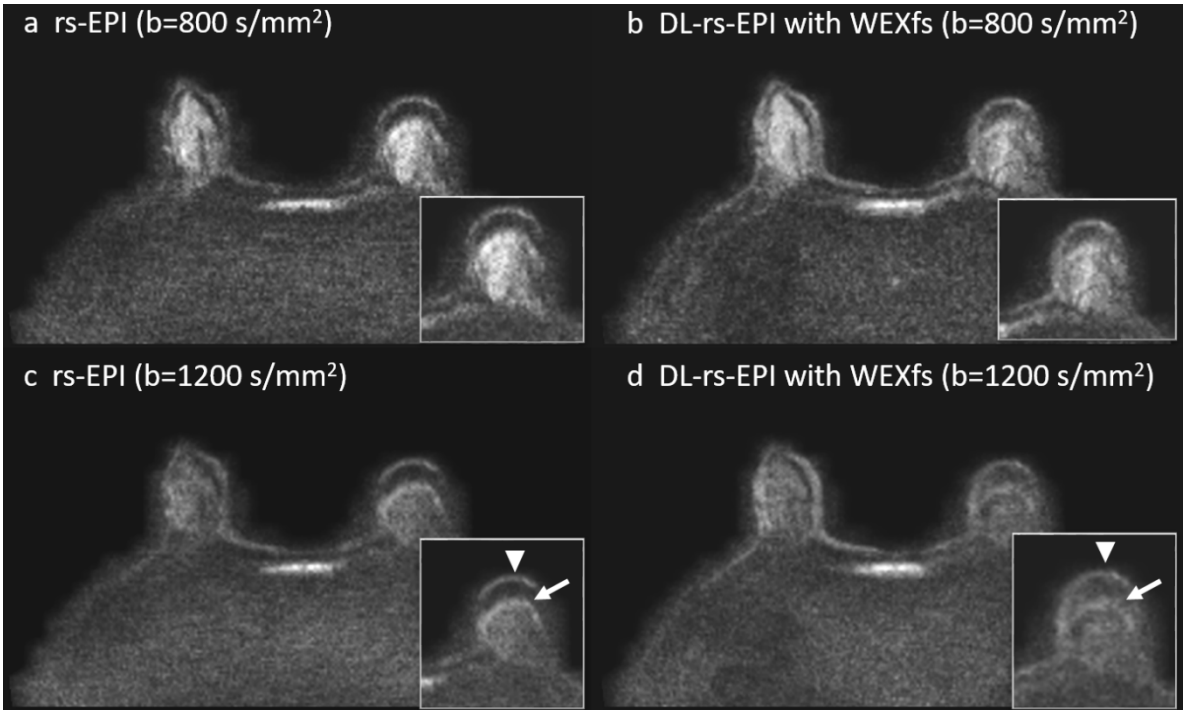

Figure 4. Breast magnetic resonance images of a 58-year-old woman with invasive ductal carcinoma in the right breast. Conventional readout-segmented echo-planar imaging (rs-EPI) images are shown in (a) and (c), while deep-learning–reconstructed readout-segmented echo-planar imaging (DL-rs-EPI) with water-excitation spectral fat suppression (WEXfs) images are shown in (b) and (d). DL-rs-EPI with WEXfs demonstrates reduced blurring and image noise compared with conventional rs-EPI. At b = 1200 s/mm², susceptibility artifact at the parenchyma–air interface (arrowheads) persists but appears less conspicuous on DL-rs-EPI with WEXfs. Similar distortion is observed at the fat–parenchyma interface (arrows), with improved lesion margin delineation on DL-rs-EPI with WEXfs.

Table 3. Results of overall qualitative analysis.

	DL-rs-EPI* **(N = 80)**	**rs-EPI *** **(N = 80)**	***p*-value**
Homogeneous fat suppression	3.80 ± 0.40	3.25 ± 0.46	<0.001
b800: background diffusion signal	2.21 ± 1.08	2.30 ± 1.06	0.008
b1200: background diffusion signal	1.27 ± 0.57	1.58 ± 0.76	<0.001
b800: lesion conspicuity	2.81 ± 0.48	2.84 ± 0.46	0.317
b1200: lesion conspicuity	2.76 ± 0.56	2.76 ± 0.56	1.000
Artifact severity	0.65 ± 0.78	0.76 ± 0.90	0.088
※ Statistical analysis method: Wilcoxon signed-rank test			

* Data represent the mean ± standard deviation of the mean qualitative scores of two readers. rs-EPI, conventional simultaneous multi-slice readout-segmented echo planar imaging; DL-rs-EPI, deep learning–based reconstruction added to rs-EPI; Inter-reader agreement for ordinal image quality scores was generally moderate to excellent (Table 4). For the background diffusion signal at b = 800 s/mm², excellent agreement was observed for both DL-rs-EPI with WEXfs (κ = 0.959, 95% CI, 0.935–0.973) and rs-EPI (κ = 0.933, 95% CI, 0.895–0.957). In contrast, lesion conspicuity demonstrated only moderate agreement for both DL-rs-EPI with WEXfs (κ = 0.684, 95% CI: 0.508–0.798) and rs-EPI (κ = 0.556, 95% CI: 0.307–0.715). A similar pattern of inter-reader agreement was observed for DWI acquired at b = 1200 s/mm².

 doi:10.20944/preprints202605.1478.v1

Table 4. Weighted kappa statistics for inter-reader agreement of qualitative image analysis.

	DL-rs-EPI	rs-EPI
Homogeneous fat suppression	0.743 (0.600–0.835)	0.491 (0.207–0.674)
b800: background diffusion signal	0.959 (0.935–0.973)	0.933 (0.895–0.957)
b1200: background diffusion signal	0.886 (0.822–0.927)	0.920 (0.876–0.949)
b800: lesion conspicuity	0.684 (0.508–0.798)	0.556 (0.307–0.715)
b1200: lesion conspicuity	0.619 (0.406–0.756)	0.575 (0.337–0.727)
Artifact severity	0.764 (0.631–0.848)	0.797 (0.684–0.870)

* Data in parentheses are 95% confidence intervals. rs-EPI, conventional simultaneous multi-slice readout-segmented echo planar imaging; DL-rs-EPI, deep learning–based reconstruction added to rs-EPI.

3.4. Quantitative Analyses: SNR, CNR, Lesion Contrast, and ADC

Compared with conventional rs-EPI, DL-rs-EPI with WEXfs demonstrated significantly higher SNR at both b-values of 800 s/mm² (5.79 ± 1.80 vs. 5.28 ± 1.74) and 1200 s/mm² (5.41 ± 1.64 vs. 4.94 ± 1.51; both $p<0.001$). CNR was likewise higher with DL-rs-EPI with WEXfs at b = 800 s/mm² (3.35 ± 1.39 vs. 3.12 ± 1.55, $p = 0.024$) and b = 1200 s/mm² (3.67 ± 1.29 vs. 3.37 ± 1.44, $p = 0.001$). Lesion contrast did not differ significantly between the two sequences at either b-value ($p>0.1$) (Table 5).

With respect to diffusion parameters, lesion ADC values were similar between the two sequences (0.96 ± 0.19 vs 0.97 ± 0.20 ×10⁻³ mm²/s, $p = 0.084$), whereas normal tissue ADC values were slightly higher with DL-rs-EPI with WEXfs (1.68 ± 0.28 vs 1.66 ± 0.26 ×10⁻³ mm²/s, $p = 0.002$). Consequently, ADC contrast was significantly greater with DL-rs-EPI with WEXfs (0.73 ± 0.31 vs 0.69 ± 0.31, $p<0.001$).

Table 5. Comparison of quantitative parameters for high *b*-value DWI with and without DL.

	Overall (n = 160)	DL-rs-EPI (n = 80)	rs-EPI (n = 80)	*p*-value
SNR				
800	5.54 ± 1.78	5.79 ± 1.80	5.28 ± 1.74	<0.001
1,200	5.17 ± 1.59	5.41 ± 1.64	4.94 ± 1.51	<0.001
CNR				
800	3.24 ± 1.47	3.35 ± 1.39	3.12 ± 1.55	0.024
1,200	3.52 ± 1.37	3.67 ± 1.29	3.37 ± 1.44	0.001
Lesion contrast				
800	3.37 ± 1.99	3.29 ± 1.64	3.45 ± 2.30	0.313
1,200	4.26 ± 2.13	4.21 ± 1.93	4.31 ± 2.32	0.513
ADC values of the lesion	0.96 ± 0.19	0.96 ± 0.19	0.97 ± 0.20	0.084
ADC values of normal FGT	1.67 ± 0.27	1.68 ± 0.28	1.66 ± 0.26	0.002
ADC contrast	0.71 ± 0.31	0.73 ± 0.31	0.69 ± 0.31	<0.001

※ Statistical analysis method: Paired t-test.
rs-EPI, conventional simultaneous multi-slice readout-segmented echo planar imaging; DL-rs-EPI, deep learning–based reconstruction added rs-EPI; SNR, signal-to-noise ratio; CNR, contrast-to-noise ratio; FGT, fibroglandular tissue; DWI, diffusion-weighted imaging

4. Discussion

In this paired, single-center cohort, a clinically implemented DL-rs-EPI with WEXfs DWI protocol demonstrated higher SNR and CNR at both b = 800 and b = 1200 s/mm² compared with a conventional rs-EPI protocol. Although rs-EPI intrinsically reduces geometric distortion compared with single-shot EPI [16], residual noise and phase inconsistencies may persist and may be exacerbated by increasing acceleration factors. Under such low-SNR conditions, reconstruction and

 doi:10.20944/preprints202605.1478.v1

fat suppression strategies that effectively suppress noise and phase-related errors are expected to provide significant benefits [17–20]. These findings are consistent with prior observations that DL-based reconstruction improves image quality, particularly under low-SNR conditions [21–23].

Most clinical studies of DL reconstruction have focused on ss-EPI or ss-EPI–based variations incorporating vendor-specific acceleration strategies by suggesting increased SNR and/or CNR and improved perceived image appearance, primarily through noise reduction while preserving ADC values [9,22–25]. One study [10] applied DL reconstruction to a multi-shot EPI technique based on MUSE at a single high b-value (b = 800 s/mm²), which segments k-space acquisition along the phase-encoding direction, in contrast to rs-EPI, with reported results consistent with observations of previous studies [10]. Moreover, all of these studies employed the SPAIR fat suppression method [9,10,22,23,25]. In this context, the present study provides evidence that DL reconstruction with WEXfs yields measurable image-quality enhancement in rs-EPI at both b = 800 and b = 1200 s/mm².

Qualitative analysis in this study demonstrated that DL-rs-EPI with WEXfs provided significant advantages in background diffusion signal (BDS) suppression at both b = 800 s/mm² (2.21 ± 1.08 vs. 2.30 ± 1.06, $p = 0.008$) and b = 1200 s/mm² (1.27 ± 0.57 vs. 1.58 ± 0.76, $p<0.001$), with a more pronounced effect observed at b = 1200 s/mm². This observation is consistent with fundamental principles of breast DWI, whereby increasing b-values lead to progressive signal attenuation in normal FGT, and the perceived BDS reflects a combination of true diffusion signal and the underlying noise floor [7,26–28]. In addition, Stephanie et al. [12] reported that WEXfs provides superior SNR and CNR at very high b-values (e.g., 1600 s/mm²) compared with lower b-values. Within this context, DL reconstruction with WEXfs, by effectively suppressing background noise and stabilizing shot-to-shot variations, is expected to have a greater impact at higher b-values. Current guidelines recommend a minimum b-value of 800 s/mm² for breast DWI [6] and propose using b-values of 0, 800, and 1200 s/mm² in screening settings [7]. In this framework, acquiring b = 800 s/mm² for quantitative ADC analysis and b = 1200 s/mm² using DL reconstruction with WEXfs to enhance lesion conspicuity and suppress background signal represents a pragmatic screening DWI strategy that improves high-b-value image quality without compromising quantitative integrity.

Lesion (tumor) ADC values remained unchanged between reconstructions, indicating no material bias in lesion diffusivity, consistent with prior reports on DL reconstruction in breast DWI [22,23]. Conversely, normal tissue ADC demonstrated an approximately 1.2% increase with DL-rs-EPI with WEXfs in vivo (1.68 ± 0.28 vs 1.66 ± 0.26 $\times 10^{-3}$ mm²/s). Importantly, phantom experiments revealed no ADC differences between DL with WEXfs and non-DL with SPAIR protocol ($p>0.1$), arguing against a systematic reconstruction-related bias [29,30]. The modest increase in normal tissue ADC observed in vivo is therefore unlikely to reflect intrinsic differences in tissue diffusivity and may instead be related to in vivo measurement-related factors, including tissue heterogeneity, intravoxel partial-volume effects, and physiologic motion, which are known to influence parenchymal ADC measurements and their reproducibility [31–33]. Furthermore, DL reconstruction has been reported to suppress background noise in low-signal regions, resulting in modest increases in ADC estimates, particularly in normal FGT with low diffusion signal intensity. Phantom studies at 3-T further support this interpretation by demonstrating that ADC bias increases under low-SNR conditions and can be mitigated by improved reconstruction and denoising, consistent with our findings of unchanged ADC in phantoms and a small, directionally explainable increase in normal tissue ADC in vivo [30].

Our qualitative item was designed to capture the homogeneity and adequacy of fat suppression, which directly influences the background signal uniformity on EPI-based breast DWI. As the two protocols employed different fat-suppression strategies (WEXfs vs SPAIR) and reconstruction methods (DL- vs. non-DL), the superior fat-suppression scores observed with DL–rs-EPI and WEXfs could be attributed to multiple factors. In DL-ss-EPI studies [8,9], no significant differences in homogeneous fat suppression have been reported; however, homogeneous fat suppression may manifest as increased SNR and CNR [34,35]. Consequently, the results of homogeneous fat suppression, SNR, and CNR may be attributed to both DL-reconstruction and WEXfs.

 doi:10.20944/preprints202605.1478.v1

This study has some limitations. First, the reconstruction method, fat suppression technique, and Repetition time (TR) differed simultaneously between the two protocols, precluding attribution of the observed differences to any single factor. Therefore, the improvements in SNR, CNR, and qualitative image quality should be interpreted as the combined effect of the overall protocol, rather than the effect of DL reconstruction alone. In addition, variations in acquisition and reconstruction parameters, including TR, fat suppression strategy, and DL-based noise suppression, may have influenced signal characteristics and quantitative measurements. In particular, the SNR estimation method may be biased by noise suppression in DL-reconstructed images. Finally, this was a retrospective, single-center study with a relatively small sample size using a single vendor system, which may limit generalizability. Further studies under controlled acquisition conditions are warranted.

5. Conclusions

In conclusion, the evaluated DL-rs-EPI DWI with WEXfs protocol demonstrated improved image quality metrics while preserving quantitative diffusion measurements, supporting the potential clinical feasibility of high-quality breast DWI protocols.

Author Contributions: Conceptualization, M.S.B. and J.H.B.; methodology, M.Y.P.; software, W.L.; validation, S.Y.L. and E.J.C. ; formal analysis, J.M.C.; investigation, J.M.C.; resources, J.M.C.; data curation, J.M.C.; writing—original draft preparation, J.M.C.; writing—review and editing, J.H.B.; visualization, W.L.; supervision, M.S.B.; project administration, J.H.B.; All authors have read and agreed to the published version of the manuscript.".

Funding: This research received no external funding.

Institutional Review Board Statement: The study was conducted in accordance with the Declaration of Helsinki and was approved by the Institutional Review Board of Ulsan University Hospital.

Informed Consent Statement: The requirement for informed consent was waived (IRB No. 2025-09-022).

Data Availability Statement: The data presented in this study are not publicly available due to privacy and ethical restrictions involving patient information. De-identified data may be available from the corresponding author upon reasonable request and subject to institutional review board approval.

Acknowledgments: During the preparation of this manuscript, the authors used ChatGPT (OpenAI, GPT-5.5) for language editing and assistance with manuscript drafting. The authors reviewed and edited the output and take full responsibility for the content of this publication.

Conflicts of Interest: The authors declare no conflicts of interest.

Abbreviations

The following abbreviations are used in this manuscript:

DWI	diffusion-weighted imaging
EPI	echo-planar imaging
DL	deep learning
ss-EPI	single-shot echo-planar imaging
rs-EPI	readout-segmented echo-planar imaging
ADC	apparent diffusion coefficient
SPAIR	spectral attenuated inversion recovery
SNR	signal-to-noise ratio
WEX	water excitation
CNR	contrast-to-noise ratio
DCE	dynamic contrast-enhanced
BDS	background diffusion signal
CI	confidence interval

 doi:10.20944/preprints202605.1478.v1

References

1. Arnold, M.; Morgan, E.; Rumgay, H.; Mafra, A.; Singh, D.; Laversanne, M.; Vignat, J.; Gralow, J.R.; Cardoso, F.; Siesling, S.; et al. Current and future burden of breast cancer: Global statistics for 2020 and 2040. *Breast* **2022**, *66*, 15–23. DOI:10.1016/j.breast.2022.08.010.
2. Bakker, M.F.; de Lange, S.V.; Pijnappel, R.M.; Mann, R.M.; Peeters, P.H.M.; Monninkhof, E.M.; Emaus, M.J.; Loo, C.E.; Bisschops, R.H.C.; Lobbes, M.B.I.; et al. Supplemental MRI screening for women with extremely dense breast tissue. *N Engl J Med* **2019**, *381*, 2091–2102. DOI:10.1056/NEJMoa1903986.
3. Heer, E.; Harper, A.; Escandor, N.; Sung, H.; McCormack, V.; Fidler-Benaoudia, M.M. Global burden and trends in premenopausal and postmenopausal breast cancer: A population-based study. *Lancet Glob Health* **2020**, *8*, e1027–e1037. DOI:10.1016/S2214-109X(20)30215-1.
4. Mann, R.M.; Cho, N.; Moy, L. Breast MRI: State of the art. *Radiology* **2019**, *292*, 520–536. DOI:10.1148/radiol.2019182947.
5. Mendez, A.M.; Fang, L.K.; Meriwether, C.H.; Batasin, S.J.; Loubrie, S.; Rodríguez-Soto, A.E.; Rakow-Penner, R.A. Diffusion breast MRI: Current standard and emerging techniques. *Front Oncol* **2022**, *12*, 844790. DOI:10.3389/fonc.2022.844790.
6. Baltzer, P.; Mann, R.M.; Iima, M.; Sigmund, E.E.; Clauser, P.; Gilbert, F.J.; Martincich, L.; Partridge, S.C.; Patterson, A.; Pinker, K.; et al. Diffusion-weighted imaging of the breast-A consensus and mission statement from the EUSOBI International Breast Diffusion-Weighted Imaging working group. *Eur Radiol* **2020**, *30*, 1436–1450.
7. Lee, S.H.; Shin, H.J.; Moon, W.K. Diffusion-weighted magnetic resonance imaging of the breast: Standardization of image acquisition and interpretation. *Korean J Radiol* **2021**, *22*, 9–22. DOI:10.3348/kjr.2020.0093.
8. Lee, E.J.; Chang, Y.W.; Lee, E.H.; Cha, J.G.; Kim, S.Y.; Choi, N.; Paek, M.; Darwish, O. Image quality and diagnostic performance of deep learning reconstruction for diffusion- weighted imaging in 3 T breast MRI. *Eur J Radiol* **2025**, *185*, 111997. DOI:10.1016/j.ejrad.2025.111997.
9. Lee, E.J.; Chang, Y.W.; Sung, J.K.; Thomas, B. Feasibility of deep learning k-space-to-image reconstruction for diffusion weighted imaging in patients with breast cancers: Focus on image quality and reduced scan time. *Eur J Radiol* **2022**, *157*, 110608. DOI:10.1016/j.ejrad.2022.110608.
10. Chien, N.; Cho, Y.H.; Wang, M.Y.; Tsai, L.W.; Yeh, C.Y.; Li, C.W.; Lan, P.; Wang, X.; Liu, K.L.; Chang, Y.C. Deep learning based multi-shot breast diffusion MRI: Improving imaging quality and reduced distortion. *Eur J Radiol* **2025**, *193*, 112419. DOI:10.1016/j.ejrad.2025.112419.
11. Quantitative Imaging Biomarkers Alliance (QIBA). QIBA Profile: Magnetic Resonance Diffusion-Weighted Imaging (DWI) of the Apparent Diffusion Coefficient (ADC); Radiological Society of North America (RSNA): Oak Brook, IL, USA, 2022.
12. Sauer, S.T.; Christner, S.A.; Schlaiß, T.; Metz, C.; Schmid, A.; Kunz, A.S.; Pabst, T.; Weiland, E.; Benkert, T.; Bley, T.A.; et al. Diffusion-weighted breast MRI at 3 Tesla: Improved lesion visibility and image quality with a combination of water-excitation and spectral fat saturation. *Acad Radiol* **2023**, *30*, 1773–1783. DOI:10.1016/j.acra.2023.01.014.
13. Hammernik, K.; Klatzer, T.; Kobler, E.; Recht, M.P.; Sodickson, D.K.; Pock, T.; Knoll, F. Learning a variational network for reconstruction of accelerated MRI data. *Magn Reson Med* **2018**, *79*, 3055–3071. DOI:10.1002/mrm.26977.
14. Bae, S.H.; Hwang, J.; Hong, S.S.; Lee, E.J.; Jeong, J.; Benkert, T.; Sung, J.; Arberet, S. Clinical feasibility of accelerated diffusion weighted imaging of the abdomen with deep learning reconstruction: Comparison with conventional diffusion weighted imaging. *Eur J Radiol* **2022**, *154*, 110428. DOI:10.1016/j.ejrad.2022.110428.
15. Liu, W.; Darwish, O.; Benkert, T.; Weiland, E.; Nickel, M.D. Improved Readout-Segmented EPI Using Deep Learning Reconstruction. Proc. Int. Soc. Magn. Reson. Med. 2024, 5106.
16. Porter, D.A.; Heidemann, R.M. High resolution diffusion-weighted imaging using readout-segmented echo-planar imaging, parallel imaging and a two-dimensional navigator-based reacquisition. *Magn Reson Med* **2009**, *62*, 468–475. DOI:10.1002/mrm.22024.

 doi:10.20944/preprints202605.1478.v1

17. Hu, Y.; Hu, Q.; Zhan, C.; Yin, T.; Ai, T. Intraobserver and Interobserver Reproducibility of Breast Diffusion-Weighted Imaging Quantitative Parameters: Readout-Segmented vs. Single-Shot Echo-Planar Imaging. *J Magn Reson Imaging* **2023**, *58*, 1725–1736. DOI:10.1002/jmri.28655.
18. Chen, N.K.; Guidon, A.; Chang, H.C.; Song, A.W. A robust multi-shot scan strategy for high-resolution diffusion weighted MRI enabled by multiplexed sensitivity-encoding (MUSE). *Neuroimage* **2013**, *72*, 41–47. DOI:10.1016/j.neuroimage.2013.01.038.
19. Filli, L.; Ghafoor, S.; Kenkel, D.; Liu, W.; Weiland, E.; Andreisek, G.; Frauenfelder, T.; Runge, V.M.; Boss, A. Simultaneous multi-slice readout-segmented echo planar imaging for accelerated diffusion-weighted imaging of the breast. *Eur J Radiol* **2016**, *85*, 274–278. DOI:10.1016/j.ejrad.2015.10.009.
20. Hancu, I.; Lee, S.K.; Hulsey, K.; Lenkinski, R.; Holland, D.; Sperl, J.I.; Tan, E.T. Distortion correction in diffusion-weighted imaging of the breast: Performance assessment of prospective, retrospective, and combined (prospective + retrospective) approaches. *Magn Reson Med* **2017**, *78*, 247–253. DOI:10.1002/mrm.26328.
21. Gudbjartsson, H.; Patz, S. The Rician distribution of noisy MRI data. *Magn Reson Med* **1995**, *34*, 910–914. DOI:10.1002/mrm.1910340618.
22. Wessling, D.; Gassenmaier, S.; Olthof, S.C.; Benkert, T.; Weiland, E.; Afat, S.; Preibsch, H. Novel deep-learning-based diffusion weighted imaging sequence in 1.5 T breast MRI. *Eur J Radiol* **2023**, *166*, 110948. DOI:10.1016/j.ejrad.2023.110948.
23. Wilpert, C.; Neubauer, C.; Rau, A.; Schneider, H.; Benkert, T.; Weiland, E.; Strecker, R.; Reisert, M.; Benndorf, M.; Weiss, J.; et al. Accelerated diffusion-weighted imaging in 3 T breast MRI using a deep learning reconstruction algorithm with superresolution processing: A prospective comparative study. *Invest Radiol* **2023**, *58*, 842–852. DOI:10.1097/RLI.0000000000000997.
24. Ming, Y.; Yang, F.; Xiao, Y.; Yue, S.; Peng, P.; Yue, X.; Pu, Q.; Yang, H.; Liang, H.; Zhang, B.; et al. Exploring the feasibility of FOCUS DWI with deep learning reconstruction for breast cancer diagnosis: A comparative study with conventional DWI. *PLOS One* **2024**, *19*, e0313011. DOI:10.1371/journal.pone.0313011.
25. Sauer, S.T.; Christner, S.A.; Lois, A.M.; Woznicki, P.; Curtaz, C.; Kunz, A.S.; Weiland, E.; Benkert, T.; Bley, T.A.; Baeßler, B.; et al. Deep learning k-space-to-image reconstruction facilitates high spatial resolution and scan time reduction in diffusion-weighted imaging breast MRI. *J Magn Reson Imaging* **2024**, *60*, 1190–1200. DOI:10.1002/jmri.29139.
26. Kang, B.J.; Kim, M.J.; Shin, H.J.; Moon, W.K. Acquisition and interpretation guidelines of breast diffusion-weighted MRI (DW-MRI): Breast imaging study group of Korean society of magnetic resonance in medicine recommendations. *Investig Magn Reson Imaging* **2022**, *26*, 83–95. DOI:10.13104/imri.2022.26.2.83.
27. Bickel, H.; Polanec, S.H.; Wengert, G.; Pinker, K.; Bogner, W.; Helbich, T.H.; Baltzer, P.A. Diffusion-weighted MRI of breast cancer: Improved lesion visibility and image quality using synthetic b-values. *J Magn Reson Imaging* **2019**, *50*, 1754–1761. DOI:10.1002/jmri.26809.
28. Christner, S.A.; Grunz, J.P.; Schlaiß, T.; Curtaz, C.; Kunz, A.S.; Huflage, H.; Patzer, T.S.; Bley, T.A.; Sauer, S.T. Breast lesion morphology assessment with high and standard b values in diffusion-weighted imaging at 3 Tesla. *Magn Reson Imaging* **2024**, *107*, 100–110. DOI:10.1016/j.mri.2024.01.005.
29. Hayashi, T.; Kojima, S.; Ito, T.; Hayashi, N.; Kondo, H.; Yamamoto, A.; Oba, H. Evaluation of deep learning reconstruction on diffusion-weighted imaging quality and apparent diffusion coefficient using an ice-water phantom. *Radiol Phys Technol* **2024**, *17*, 186–194. DOI:10.1007/s12194-023-00765-8.
30. Lemainque, T.; Yoneyama, M.; Morsch, C.; Iordanishvili, E.; Barabasch, A.; Schulze-Hagen, M.; Peeters, J.M.; Kuhl, C.; Zhang, S. Reduction of ADC bias in diffusion MRI with deep learning-based acceleration: A phantom validation study at 3.0 T. *Magn Reson Imaging* **2024**, *110*, 96–103. DOI:10.1016/j.mri.2024.04.018.
31. Dkhar, W.; Kadavigere, R.; Mustaffa, S.P.; Pradhan, A.; Ravichandran, S.; Barnes, N.A. Impact of breast density and menopausal status on apparent diffusion coefficient values of the breast tissues in diffusion-weighted MRI. *Bratisl Med J* **2025**, *126*, 3138–3147. DOI:10.1007/s44411-025-00313-3.
32. Partridge, S.C.; Singer, L.; Sun, R.; Wilmes, L.J.; Klifa, C.S.; Lehman, C.D.; Hylton, N.M. Diffusion-weighted MRI: Influence of intravoxel fat signal and breast density on breast tumor conspicuity and apparent diffusion coefficient measurements. *Magn Reson Imaging* **2011**, *29*, 1215–1221. DOI:10.1016/j.mri.2011.07.024.

 doi:10.20944/preprints202605.1478.v1

33. Rahbar, H.; Kurland, B.F.; Olson, M.L.; Kitsch, A.E.; Scheel, J.R.; Chai, X.; Usoro, J.; Lehman, C.D.; Partridge, S.C. Diffusion-weighted breast magnetic resonance imaging: A semiautomated voxel selection technique improves interreader reproducibility of apparent diffusion coefficient measurements. *J Comput Assist Tomogr* **2016**, *40*, 428–435. DOI:10.1097/RCT.0000000000000372.
34. Chen, Z.; Xing, Z.; Zheng, E.; Luo, M.; Fu, C.; Li, G.; Benkert, T.; Xue, Y.; Sun, B. Optimization of motion-corrected liver diffusion-weighted imaging at 3 Tesla (3T): Incorporating complex averaging and reparametrized sinc fatsat pulse with optimized water excitation pulse. *Quant Imaging Med Surg* **2024**, *14*, 6579–6589. DOI:10.21037/qims-24-340.
35. Liu, X.; Yang, L.; Zhang, Y.; Hu, S.; Hu, Y.; Sun, R.; Qin, M.; Chen, J.; Zhang, X.; Yin, T.; et al. Enhanced diagnostic performance of WE-SHARP-DWI compared with SPAIR-DWI for focal liver lesion evaluation at 3T. *Abdom Radiol* **2025**, *51*, 1880–1894. DOI:10.1007/s00261-025-05189-z.